Alternative Catalytic Anions Differentially Modulate Human α-Amylase Activity and Specificity[†,‡]

Robert Maurus,[§,||] Anjuman Begum,[§,||] Leslie K. Williams,[§] Jason R. Fredriksen,[§] Ran Zhang,[⊥] Stephen G. Withers,[§,⊥] and Gary D. Brayer*[,§]

Department of Biochemistry and Molecular Biology, University of British Columbia, Vancouver, British Columbia V6T 1Z3, Canada, and Department of Chemistry, University of British Columbia, Vancouver, British Columbia V6T 1Z1, Canada

Received August 15, 2007; Revised Manuscript Received November 17, 2007

ABSTRACT: A mechanistic study of the essential allosteric activation of human pancreatic α-amylase by chloride ion has been conducted by exploring a wide range of anion substitutions through kinetic and structural experiments. Surprisingly, kinetic studies indicate that the majority of these alternative anions can induce some level of enzymatic activity despite very different atomic geometries, sizes, and polyatomic natures. These data and subsequent structural studies attest to the remarkable plasticity of the chloride binding site, even though earlier structural studies of wild-type human pancreatic α-amylase suggested this site would likely be restricted to chloride binding. Notably, no apparent relationship is observed between anion binding affinity and relative activity, emphasizing the complexity of the relationship between chloride binding parameters and the activation mechanism that facilitates catalysis. Of the anions studied, particularly intriguing in terms of observed trends in substrate kinetics and their novel atomic compositions were the nitrite, nitrate, and azide anions, the latter of which was found to enhance the relative activity of human pancreatic α-amylase by nearly 5-fold. Structural studies have provided considerable insight into the nature of the interactions formed in the chloride binding site by the nitrite and nitrate anions. To probe the role such interactions play in allosteric activation, further structural analyses were conducted in the presence of acarbose, which served as a sensitive reporter molecule of the catalytic ability of these modified enzymes to carry out its expected rearrangement by human pancreatic α-amylase. These studies show that the largest anion of this group, nitrate, can comfortably fit in the chloride binding pocket, making all the necessary hydrogen bonds. Further, this anion has nearly the same ability to activate human pancreatic α-amylase and leads to the production of the same acarbose product. In contrast, while nitrite considerably boosts the relative activity of human pancreatic α-amylase, its presence leads to changes in the electrostatic environment and active site conformations that substantially modify catalytic parameters and produce a novel acarbose rearrangement product. In particular, nitrite-substituted human pancreatic α-amylase demonstrates the unique ability to cleave acarbose into its acarviosine and maltose parts and carry out a previously unseen product elongation. In a completely unexpected turn of events, structural studies show that in azide-bound human pancreatic α-amylase, the normally resident chloride ion is retained in its binding site and an azide anion is found bound in an embedded side pocket in the substrate binding cleft. These results clearly indicate that azide enzymatic activation occurs via a mechanism distinct from that of the nitrite and nitrate anions.

Human pancreatic α-amylase (α-1,4-glucan-4-glucanohydrolase, EC 3.2.1.1) is an endoglycosidase, which hydrolyzes starch and related α-1,4-linked glycosyl polysaccharides. Related enzymes are found in many organisms, although the primary sequences of these show little sequence homology. Nonetheless, the folded structures of these enzymes are found to be remarkably conserved in organisms ranging from microbes to mammals. Particularly prominent is the common presence of three domains. Domain A consists of an α/*β*-barrel and contains the active site; domain B protrudes from the side of domain A and contains the calcium binding site, and domain C forms a structurally independent antiparallel *β*-barrel (*2*–*7*).

Substantial effort has been directed at elucidating the catalytic mechanism of this family of enzymes (*8*–*11*). Human pancreatic α-amylase (HPA)[1] and related α-amylases are found to be retaining glycosidases, catalyzing substrate hydrolysis by a double-displacement mechanism whereby a

[†] This work was supported by an operating grant from the Canadian Institutes of Health Research (CIHR).

[‡] Coordinate and structure factor files for the human pancreatic α-amylase structures described in this work have been deposited in the Protein Data Bank (*1*). The following PDB file names have been assigned: 2QMK for the nitrite complex, 2QV4 for the nitrite−acarbose complex, 3BAI for the nitrate complex, 3BAJ for the nitrate−acarbose complex, 3BAK for the N298S variant with nitrate complex, 3BAY for the N298S variant with the nitrate−acarbose complex, 3BAW for the azide complex, and 3BAX for the N298S with azide complex.

* To whom correspondence should be addressed. Telephone: (604) 822-5216. Fax: (604) 822-5227. E-mail: brayer@interchange.ubc.ca.

[§] Department of Biochemistry and Molecular Biology.

[||] These authors contributed equally to this work.

[⊥] Department of Chemistry.

[1] Abbreviations: HPA, human pancreatic α-amylase; αG3F, α-maltotriosyl fluoride; αCNP-G3, 2-chloro-4-nitrophenyl α-maltotrioside; rms, root-mean-square. The amino acid numbering is according to a sequence alignment of HPA (*2*).

10.1021/bi701652t CCC: $40.75
Published on Web 02/20/2008

covalent glycosyl−enzyme intermediate is formed and hydrolyzed through oxocarbenium ion-like transition states (*12, 13*). A required feature of this mechanism is the presence of two carboxylic acid-containing side chains in the active site of the enzyme. One of these carboxylic acids (D197 in HPA) acts as the catalytic nucleophile and displaces the aglycon portion of the substrate upon formation of the covalent intermediate. The other carboxylic acid acts as the acid/base catalyst (E233 in HPA) and thereby assists in the stabilization of the two transition states proposed to occur in the hydrolysis process. For HPA, D300 is a third catalytic residue that plays a critical role in stabilizing the conformation of bound substrates (*11, 14*).

Some members of this family of enzymes, including human pancreatic α-amylase (HPA), are allosterically activated by chloride (*15*). Chloride binding modulates the maximal activity and pH optima of these enzymes (*15–20*). The intestinal environment in which HPA functions is relatively abundant in chloride ions (*21*). Contributing fluids with substantial chloride ion content include gastric juices (150 mM), bile (50 mM), and pancreatic excretions (30 mM). Structural studies have delineated the structural determinants and detailed interactions that form the chloride ion binding site in HPA (*2, 15*). Three residues play a direct role in binding chloride ion and include R195, N298, and R337. Notably, the side chain of R195 is also directly hydrogen bonded to the side chain of the catalytic nucleophile D197, as well as to the side chain of E233, which functions as the acid/base catalyst (*10*). Furthermore, R195 along with H299 and D300 forms hydrogen bonds to the substrate glucose ring bound in the −1 binding subsite, and it is this glucose moiety that is attacked by the catalytic nucleophile during enzymatic hydrolysis (*22*). Further removed from the active site is the N298 ligand of bound chloride. The side chain of this residue also binds to a water molecule that may play the role of nucleophile in the cleavage of the covalent intermediate formed during catalysis. The third chloride binding ligand is R337, which is more remotely located at the bottom of the chloride ion binding pocket.

As part of previous studies of human pancreatic α-amylase, we have carefully examined the roles of the positively charged chloride ligands R195 and R337, through a structure–function−mutagenesis approach (*15*). For the series of substitutions R195A, R195Q, R337A, and R337Q, no chloride binding could be detected, and structural analyses confirmed this finding while also showing that the overall structure of HPA was not perturbed. However, these variant proteins did have different kinetic properties. The most pronounced differences involved the R195 variants, with activities 20–450-fold lower than that of the wild type and pH optima shifted to a more basic pH. More modest kinetic changes were observed for the R337 variants (2-fold), and interestingly, neither variant was chloride-dependent. Collectively, these results demonstrated that R337 and R195 are both involved in the binding of chloride ion, with R195 also playing a key role in transition state stabilization.

In further studies, we have examined HPA in both the presence and absence of chloride ion, using the N298S variant enzyme, which has a chloride dissociation constant of 162 mM (compared to 0.52 mM for wild-type HPA), nicely fitting into a range that facilitated both kinetic and structural analyses (*23*). Kinetic studies clearly demonstrated the pronounced activating effect of chloride ion binding on reaction rates and its effect on the pH dependence of catalysis. Conformational shifts observed in the N298S variant upon chloride ion binding suggest that the chloride ion plays a variety of roles that serve to promote catalysis. One of these is having a strong influence on the positioning of the acid/base catalyst residue E233. Chloride ion and N298 also appear to stabilize a helical region of polypeptide chain from which projects the flexible substrate binding loop unique to chloride-dependent α-amylases. This structural feature also serves to properly orient the catalytically essential residue D300.

Our current experimental efforts are directed at obtaining a more comprehensive understanding of how chloride itself functions to allosterically enhance catalytic activity, by binding substitute alternative anions with differing chemical properties into the chloride binding site. The major goals are to assess the degree of flexibility that is available to bind alternative anions, whether alternative anions alter active site residue conformations, catalytic properties, cleavage preferences, and resultant product profiles, and whether the observed differences can assist in improving our understanding of the unique allosteric properties of the chloride anion. Notably, HPA is an important enzyme in the control of blood glucose levels and is therefore an attractive target in the search for new inhibitors for therapeutic applications related to diabetes and obesity. Unfortunately, there are no known inhibitors of HPA having both of the properties of high specificity and binding affinity. A further goal of this study is to gain sufficient information about the properties of the chloride binding pocket to assess the possibility of incorporating this structural feature into the design of a new class of inhibitors uniquely specific for HPA.

EXPERIMENTAL PROCEDURES

Materials. All buffer chemicals and reagents were obtained from Sigma/Aldrich Canada unless otherwise noted. 2-Chloro-4-nitrophenyl α-maltotrioside (αCNP-G3) was a kind gift from GelTex Pharmaceuticals.

Bacterial Strain, Media, and Plasmids. Escherichia coli DH5R subcloning efficiency competent cells were obtained from Gibco BRL Products and were used for all transformations and DNA manipulations according to standard procedures (*24*). *Pichia pastoris* strain GM5011 was used for the expression of wild-type and N298S proteins. Growth and expression media were prepared as published in the *Pichia* expression kit (Invitrogen). The construction of the expression vectors for wild-type HPA (pPIC9-AMY) and the N298S variant of HPA (pPIC9-AMY-N298S) was described previously (*10, 15*).

HPA Expression and Purification. Transformation of HPA plasmids into *P. pastoris* cells and subsequent selection were carried out according to directions in the *Pichia* expression kit (Invitrogen) and as described previously (*10, 15*). Wild-type and variant HPAs were deglycosylated and purified through the use of phenyl-Sepharose and Q-Sepharose columns (Pharmacia). The mass and purity of isolated protein samples were confirmed by electrospray mass spectrometry and SDS−PAGE. Enzyme concentrations were determined spectrophotometrically by using an $A^{0.1\%}$ of 2.2 at 280 nm for both wild-type and N298S variant HPAs. Detailed

Table 1: Summary of Diffraction Data Collection and Structural Refinement Statistics

	WT + NO_2^-	WT + NO_2^- + acarbose	WT + NO_3^-	WT + NO_3^- + acarbose	N298S + NO_3^-	N298S + NO_3^- + acarbose	WT + N_3^-	N298S + N_3^-
Data Collection								
space group	$P2_12_12_1$	$P2_12_12_1$	$P2_12_12_1$	$P2_12_12_1$	$P2_12_12_1$	$P2_12_12_1$	$P2_12_12_1$	$P2_12_12_1$
unit cell dimensions (Å)								
a	51.7	51.8	53.0	53.1	52.4	52.2	51.8	52.1
b	67.6	67.7	69.1	69.2	69.0	68.9	67.4	67.8
c	129.4	130.1	132.2	132.7	131.3	131.2	129.7	130.1
no. of unique reflections	16852	32323	39142	29386	38506	31287	30454	36630
mean $I/\sigma I$[a]	19.5 (8.6)	42.5 (14.0)	21.7 (4.1)	13.7 (2.5)	26.4 (13.8)	21.5 (3.6)	16.4 (3.1)	34.2 (16.8)
multiplicity[a]	2.4 (2.0)	4.5 (3.8)	6.8 (4.8)	4.8 (3.1)	7.5 (6.3)	3.0 (2.4)	6.5 (1.9)	7.1 (6.7)
merging *R*-factor (%)[a]	6.3 (17.8)	4.0 (11.7)	6.2 (30.4)	9.7 (35.2)	5.4 (14.3)	6.0 (29.9)	3.4 (13.5)	3.6 (11.3)
maximum resolution (Å)	2.30	1.97	1.90	2.10	1.90	1.99	2.00	1.90
Structure Refinement								
no. of reflections	16454	30932	38413	28163	37873	31168	30399	33829
resolution range (Å)	30–2.30	30–1.97	30–1.9	30–2.1	30–1.9	30–1.99	30–2.0	30–1.9
completeness (%)[a]	80.7 (72.6)	97.5 (91.3)	98.3 (92.2)	96.0 (84.6)	98.6 (85.9)	93.8 (86.1)	96.7 (87.4)	91.1 (79.6)
no. of protein atoms	3945	3945	3945	3945	3943	3943	3945	3943
no. of water molecules	270	410	361	283	319	235	528	616
no. of inhibitor atoms	−	55	−	55	−	55	−	−
average thermal factors (Å^2)								
protein atoms	27.2	19.6	25.6	27.9	23.2	35.3	13.6	16.9
activating anion	33.4	17.4	27.6	28.8	34.2	35.1	10.7	26.1
acarbose ligand	−	86.3	−	66.9	−	74.6	−	−
water molecules	32.9	33.6	42.6	41.1	38.4	45.8	32.4	36.1
final *R*-factor/R_{free} (%)[b]	17.2/21.8	17.6/22.4	16.9/19.2	17.7/21.2	17.5/18.2	18.8/22.3	16.3/21.4	15.5/19.0
Structure Stereochemistry								
bonds (Å)	0.007	0.007	0.005	0.006	0.006	0.006	0.007	0.006
angles (deg)	1.3	1.5	1.1	1.05	1.09	1.05	1.37	1.05

[a] Values in parentheses refer to the highest-resolution shell: 2.07–2.00 Å for the WT + N_3^- structure, 2.02–1.97 Å for the WT + NO_2^- + acarbose structure, 1.93–1.90 Å for the WT + NO_3^-, N298S + NO_3^-, and N298S + N_3^- structures, 2.03–1.99 Å for the N298S + NO_3^- + acarbose structure, 2.34–2.30 Å for the WT + NO_2^- structure, and 2.14–2.10 Å for the WT + NO_3^- + acarbose structure. [b] Five percent of the data was set aside to calculate R_{free}.

purification protocols for human pancreatic α-amylase can be found in refs *10*, *15*, and *23*.

Kinetic Studies. Standard assays for the wild-type and N298S variant HPAs were carried out at 30 °C in 20 mM sodium phosphate buffer (pH 6.0) using 2.0 mM CNP-G3 as the substrate. For these measurements, concentrations of 10 and 300 mM NaCl were maintained in wild-type and variant solutions, respectively, unless otherwise stated. For anion substitution studies, purified enzyme (wild-type and N298S variant) was first buffer-exchanged three times against 20 mM phosphate buffer (pH 7.0) by ultrafiltration using Amicon Centripreps to remove residual chloride. Hydrolysis of CNP-G3 was followed by measurement of the increase in absorbance at 400 nm using a Varian CARY 4000 spectrophotometer attached to a temperature control unit. Kinetic data obtained on the dependence of wild-type and variant HPA activities on different anions were fit to a ligand binding equation by nonlinear regression using GraFit version 4.0.21 (*25*). For the nitrate, nitrite, and azide anions, further analyses of the pH dependence of wild-type and variant HPA activities were conducted by varying the pH of the sodium phosphate buffer. Plots of pH versus activity were fit to a double-ionization pH curve by nonlinear regression using GraFit version 4.0.21.

Structure Determinations. Recombinant wild-type and N298S variant HPAs were crystallized using the hanging drop vapor diffusion method (*22, 26*). The reservoir solution contained 60% 2-methylpentane-2,4-diol and 100 mM cacodylate (pH 7.5), and the hanging drops consisted of 5 μL of protein solution (16.3 mg/mL) mixed with 5 μL of reservoir solution. Diffraction quality crystals appeared over the period of a month. The normally resident catalytic chloride ion was displaced from these crystals when they were soaked in the crystallization reservoir solution in the presence of 300 mM $NaNO_3$ or with 400 mM $NaNO_2$ for 20 min. Crystals of the NaN_3 (300 mM) complex were formed in a similar manner. Crystals of complexes of HPA with acarbose were prepared by being soaked for 20 min in the same crystallization reservoir and anion solutions described above, with the addition of 100 mM acarbose.

Diffraction data for all anion-substituted and acarbose-complexed crystals of wild-type and N298S variant HPAs were collected on a Mar 345 imaging plate area detector system at 100 K, using Cu Kα radiation supplied by a Rigaku RU300 rotating anode generator operating at 50 kV and 100 mA. The diffraction data obtained were processed and reduced with the HKL software package (*27*). The resultant data collection statistics are listed in Table 1.

Since crystals of all anion-substituted and acarbose-complexed wild-type HPAs were isomorphous with that of wild-type HPA, the structure of the latter (*2*) was used as the starting refinement model, with the normally bound chloride ion and solvent molecules removed. Similarly, the previously determined structure of the N298S variant of HPA (*23*) served as the starting model for nitrate-substituted and acarbose-complexed structures of this protein. Refinements were carried out with the CNS software package (*28*). Positional and individual atom isotropic *B*-factor refinement were alternated, and where necessary, the refinement model was manually rebuilt. In the initial stages of structural

refinements, the complete polypeptide chain of the refinement model was examined and adjusted on the basis of omit maps (with 10 residues omitted per segment). Subsequently, the complete polypeptide chain was examined periodically with $F_o - F_c$ and $2F_o - F_c$ difference electron density maps. Following refinement of the polypeptide chain of HPA, alternatively bound anions and bound acarbose products were positioned on the basis of $F_o - F_c$ difference electron density maps. For all complexes, protein, anion, and inhibitor atoms were then jointly refined to obtain the best overall fit. In addition, an *N*-acetylglucosamine moiety was built into observed electron density and refined, to reflect glycosylation of N461 in all complexes. At this point, water molecules were identified from another $F_o - F_c$ difference electron density map and included in the refinement model if these were able to hydrogen bond to protein atoms and refined with a thermal factor of less than 75 Å^2. All protein, anion, inhibitor, and water molecules were then jointly refined to convergence. The final refinement statistics obtained are detailed in Table 1.

RESULTS

HPA Activation Properties with Different Anions. HPA is essentially inactive in the absence of chloride ion. This anion allosterically activates HPA and modulates the pH optimum for hydrolytic activity (*15, 23*). Chloride is found bound in a well-defined pocket buried just below the surface of the active site binding cleft near the catalytic residues D197, E233, and D300 (*2*). The strong affinity of HPA for chloride ion (K_d = 0.48 mM) makes it difficult to study, and a very useful probe of its function has turned out to be the N298S variant of this enzyme, which has an approximate 200-fold reduction in affinity for chloride ion (91 mM), allowing the study of this enzyme with or without bound chloride. Notably, unlike removal of the R195 and R337 chloride liganding residues, substitution at the N298 ligand by serine does not abolish chloride binding or the dependence of enzyme activity on chloride concentration (*23*).

To further probe the specificity and mechanistic features of chloride binding to HPA, as well as assess its impact on product formation, we have explored a wide range of possible anion substitutions that have the potential to bind at the chloride site. These studies have included not only different halides but also alternative monovalent and divalent anions of differing chemical composition, planarity, and size. As Table 2 shows, a rather surprising result of these studies is that of the 12 diverse anions tested, eight were found to induce some level of enzymatic activity at saturating levels in solution, despite having characteristics very different from those of the naturally bound chloride anion. This is even more remarkable given our earlier studies, which documented the rather precise space requirements and ligand interactions that occur in the chloride binding site (*15*). Clearly, this site has greater plasticity than would be indicated from previous structural studies alone.

As Table 2 shows, among substitute halides, the fluoride anion was found to be inactive. However, bromide anion has a greater affinity for HPA than chloride and a comparable relative activity, whereas iodide anion, although having a much poorer affinity for HPA, actually increased the relative hydrolytic activity. These results suggest that despite its larger size bromide can comfortably and efficiently substitute for chloride ion, but that the much larger iodide anion has trouble fitting within the available chloride binding pocket space.

Table 2: Activation Properties of Different Classes of Anions on Human α-Amylase[a]

	WT		N298S	
anion	relative activity (%)	K_d (mM)	relative activity (%)	K_d (mM)
Cl^-	100	0.48	100	90
Br^-	105	0.20	73	19
I^-	165	13.5	62	19
F^-	NME	−	NME	−
NO_3^-	103	0.80	135	39
NO_2^-	157	2.9	212	190
N_3^-	496	37	545	440
ClO_3^-	90	0.47	96	41
$HCOO^-$	105	495	133	3600
SCN^-	41	0.10	26	825
CH_3COO^-	NME	−	NME	−
SO_4^-	NME	−	NME	−
HCO_3^-	NME		NME	−

[a] Anions are present at saturation; enzyme activity was measured with CNP-G3 as the substrate. NME refers to no measurable effect.

A particularly interesting result arising from Table 2 is the ability of the nitrate, nitrite, and azide anions to bind to HPA in light of their unique geometries and multiatom compositions. Especially noteworthy is the influence of the linear azide anion, which boosted the relative enzymatic activity by nearly 5-fold, even though it demonstrated a rather poor binding affinity for HPA. Remarkably, the larger planar groupings of the nitrate and nitrite anions proved to be reasonable substitutes for chloride with, for example, the binding affinity for nitrate being reduced to only approximately half of that of chloride and yet inducing a comparable level of relative enzymatic activity. Interestingly, nitrite anion substitution actually substantially increased activity in the face of a somewhat weaker binding affinity for HPA.

The equally novel anions chlorate, thiocyanate, and formate, with their unique geometry and composition, also exhibited comparable or somewhat lower relative activities. The ability of chlorate ion to bind with nearly the same affinity as chloride is unexpected given the much larger size of this anion, which has a partial molal ionic volume in the range of 39 mL/mol versus 18 mL/mol for chloride (*29, 30*). This is likely attributable to the placement of chlorate ion oxygens in side depressions in the chloride binding pocket, in much the same manner that occurs for bound nitrite and nitrate anions. This is supported by the observation that the iodide anion, with a comparable partial molal ionic volume of 37 mL/mol, but a spherical geometry, has a much poorer affinity for the chloride binding site, since it is unable to readily take advantage of the available open spaces. Of the anions promoting HPA catalysis, thiocyanate and formate are found to be at the extremes of binding affinity, with the thiocyanate being the strongest with a K_d of 0.1 mM and formate the weakest with a K_d of 495 mM. As Table 2 indicates, the acetate, carbonate, and sulfate anions show no activity with HPA and are presumably examples of anions that are too large or stereochemically incompatible to be accommodated in the chloride binding site.

Reflecting the loss of a potential ligand interaction, different anion activation trends appear in the N298S variant

of HPA (Table 2). In wild-type HPA, the terminal side chain amide ND2 forms a direct ligand bond to bound chloride. This same ND2 group hydrogen bonds to a water molecule, which in turn is hydrogen bonded to catalytic residues E233 and D300 (*23*). In the N298S variant protein, a substantially different hydrogen bonded network is present, with the side chain hydroxyl of S298 interacting with bound chloride through a water molecule. This new water is roughly positioned where ND2 in the side chain of N298 in the wild-type enzyme is located. Substitution of S298 also greatly increases the overall volume available in the anion binding pocket of HPA, and this, in concert with the loss of a direct liganding interaction, would appear to account for the ~200-fold loss of binding affinity for chloride ion.

In a reversal of a trend observed for the wild-type protein, the bromide and iodide ion replacements have lower relative activities in the N298S variant, despite the smaller impact that the absence of the N298 ligand has had on binding affinity when compared to chloride ion (Table 2). Therefore, for the bromide and iodide ions, it would seem ligand formation is of primary importance and the absence of N298 compromises their functionality in HPA activation to a greater extent than for chloride ion. As Table 2 demonstrates, for these halides and the other anions that were studied, there is no apparent relationship between binding affinity and relative activity.

A rather different trend occurs with the nitrate, nitrite, and azide series of anions. Unlike what is seen with increasing halide size, in the N298S variant protein these anions show substantially increasing relative activities, even though there is also a significant loss of binding affinity, ranging from ~50-fold for nitrate to ~10-fold for azide. This suggests that the larger volume of the N298S variant anion binding pocket is advantageous in promoting a more optimal orientation of these anions when bound, thereby facilitating substrate hydrolysis. This trend in larger anion response to N298S substitution continues with the chlorate, thiocyanate, and formate anions. For these anions, much lower binding affinities are observed (~8000-fold for thiocyanate), whereas overall relative activities are comparable or slightly increased. However, as Table 2 shows, it would seem that the acetate, sulfate, and HCO_3^- ions are too large to fit the chloride binding pockets of either wild-type or N298S HPA.

Substrate Kinetic Parameters in the Presence of Different Anions. Of the anions examined in Table 2, those having the highest relative activities were further investigated in terms of their impact on kinetic parameters in the hydrolysis of the substrate CNP-G3 by wild-type and N298S variant HPAs. Curves of initial rate versus substrate concentration obtained for these anions at their optimal concentrations are presented in Figure 1. Analysis of experimentally observed rates was performed using the general Michaelis–Menten initial velocity equation for the determination of k_{cat} and K_m. Kinetic values obtained for each anion substitution are given in Table 3.

For wild-type HPA, these results show that the larger halide anions (bromide and iodide) have a negative influence on substrate K_m values, leading to values of k_{cat}/K_m that are half of those obtained for the normally resident chloride ion. In contrast, the nitrate, nitrite, and azide anion series had lower substrate K_m values, with k_{cat} values for nitrate and nitrite in the range of that of the chloride ion. Particularly

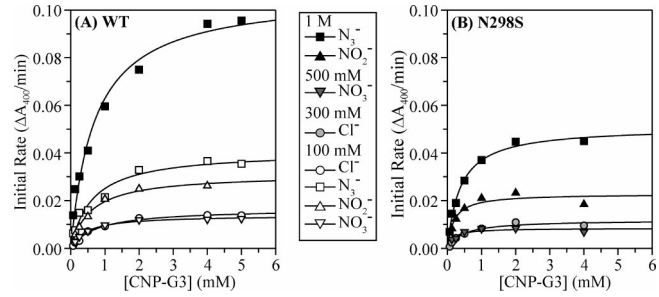

FIGURE 1: Michaelis–Menten kinetic curves showing the effect of various monovalent anions on the rate of cleavage of CNP-G3 by (A) wild-type and (B) N298S variant HPA. As identified in the central box legend, a plotted curve is presented for the optimal concentration of each anion, with the exception of azide, where an additional lower-concentration curve is drawn for wild-type HPA.

Table 3: Kinetic Parameters for Hydrolysis of CNP-G3 by Wild-Type and N298S Variant (values in parentheses) HPA in the Presence of Different Activating Anions at the Optimal Concentration

anion	optimum anion concentration (M)	K_m (mM)	k_{cat} (s^{-1})	k_{cat}/K_m (mM^{-1} s^{-1})
Cl^-	0.01 (0.30)	0.76 (0.45)	2.4 (0.86)	3.2 (1.5)
Br^-	0.10 (0.40)	1.2 (0.35)	1.9 (0.63)	1.6 (1.8)
I^-	0.10 (0.20)	1.3 (0.61)	2.1 (0.39)	1.5 (0.64)
NO_3^-	0.10 (0.50)	0.45 (0.16)	2.2 (0.63)	4.9 (3.8)
NO_2^-	1.00 (1.00)	0.58 (0.19)	3.5 (1.70)	5.1 (8.9)
N_3^-	1.00 (1.00)	0.69 (0.37)	15.8 (3.80)	22.9 (10.3)
ClO_3^-	0.20 (0.50)	0.58 (0.22)	2.0 (0.38)	3.4 (1.7)
$HCOO^-$	1.00 (0.60)	0.57 (0.09)	4.4 (0.42)	7.8 (4.8)

noteworthy, however, is the ~5-fold increase in k_{cat} observed for the azide ion, leading to the highest k_{cat}/K_m value obtained for any of the anions studied. Substrate binding in the case of the chlorate and formate ions was comparable with that seen in the presence of chloride ion, as was the value for k_{cat}/K_m for chlorate, whereas this parameter was ~2-fold higher for the formate ion.

It is evident from both Tables 2 and 3 that the substitution of a shorter serine side chain for N298 significantly impacts the ability of HPA to bind different anions in the now much larger anion binding pocket and thereby substantially affects substrate kinetic hydrolysis parameters. For the halide series, while optimum anion concentrations are much higher, substrate K_m values are lower and similar to that seen in the presence of chloride ion. Uniquely, the iodide ion yields an enzyme with a low k_{cat} value and a k_{cat}/K_m value less than half that of the chloride and bromide values. This halide pattern of influence on substrate kinetics is quite different than that observed for wild-type HPA. Notably, for the nitrate, nitrite, and azide anions, significantly lower substrate K_m values were observed, leading to much larger k_{cat}/K_m values, ranging from ~2-fold higher for nitrate ion to ~7-fold for the azide anion. These results suggest that the larger anion binding pocket space available in the N298S variant HPA allows these anions to achieve more optimal fits in this region and that this facilitates the process of substrate binding and hydrolysis. For the chlorate and formate ions, a similar lower trend in substrate K_m is observed, but in these cases, observed k_{cat} values are also lower, overall giving a k_{cat}/K_m value in the range of that seen in the presence of chloride for the chlorate ion and ~3-fold higher for the formate ion. Collectively, wild-type and N298S substrate kinetic data emphasize the interplay and complexity of anion binding

Table 4: pK_a Values Obtained from k_{cat}/K_m versus pH Dependence Curves of Wild-Type and N298S HPA at Different Anion Concentrations

HPA	anion	concentration (mM)	pK_{a1}	pK_{a2}
wild-type	Cl^-	0.00	5.7	6.7
		0.25	6.0	6.8
		5.00	6.0	7.3
		10.0	6.1	7.6
		100	6.0	8.2
	NO_3^-	10.0	4.6	7.4
		50.0	5.1	7.0
		100	5.6	6.9
	NO_2^-	10.0	5.5	7.9
		50.0	5.3	7.7
		1000	5.0	7.6
	N_3^-	1.00	5.2	6.6
		10.0	3.6	6.7
		100	4.4	6.7
		500	4.3	7.0
		1000	4.0	7.2
N298S	Cl^-	10.0	4.2	6.0
		100	4.3	6.2
		300	4.4	7.4
		600	5.4	7.9
	NO_3^-	10.0	4.8	6.4
		100	6.4	7.0
		200	6.8	7.3
	NO_2^-	10.0	4.7	7.8
		100	6.0	6.6
		500	6.0	6.6
	N_3^-	10.0	4.3	7.8
		100	4.3	7.1
		300	4.1	6.8
		600	3.9	6.5

parameters (pocket size, anion composition and geometry, and potential ligand interactions) with respect to the activation mechanism employed by these anions in the process of substrate binding and hydrolysis.

pH Dependency of Nitrate, Nitrite, and Azide Activation. Of the anions studied, particularly intriguing in terms of observed trends in substrate kinetics and their novel atomic geometries and polyatomic compositions are the nitrate, nitrite, and azide anions. To further understand how these anions can apparently substitute for chloride in the catalytic mechanism of HPA, their complexes were investigated with regard to pH dependency. The dependence of wild-type HPA activity on pH has been determined in earlier studies in the presence of a range of chloride concentrations and found to result in a bell-shaped curve (*15*). The simplest explanation of this result is that two ionizations are observed, associated with the catalytic nucleophile (D197-acid limb) and the acid/base catalyst (E233-basic limb). In the current (Table 4) and previous studies (*23*), pK_{a1} is largely independent of chloride concentration. This is consistent with the fact that D197 is removed from the direct vicinity of the chloride binding site (*22*). However the value of pK_{a2} is closely tied to chloride concentration, likely due to the proximity of the catalytic residue E233 to bound chloride.

Anion-substituted HPAs also exhibit a bell-shaped dependence of pH on anion concentration, but in a direct reflection of their unique geometries and charge distributions, these anions also have a substantial impact on observed pK_{a1} and pK_{a2} values (see Table 4 and Figure 2). For nitrate, nitrite, and azide, there is a clear trend toward lower values for both of these parameters, indicating a larger impact on both the nearby E233 and the more remote catalytic nucleophile

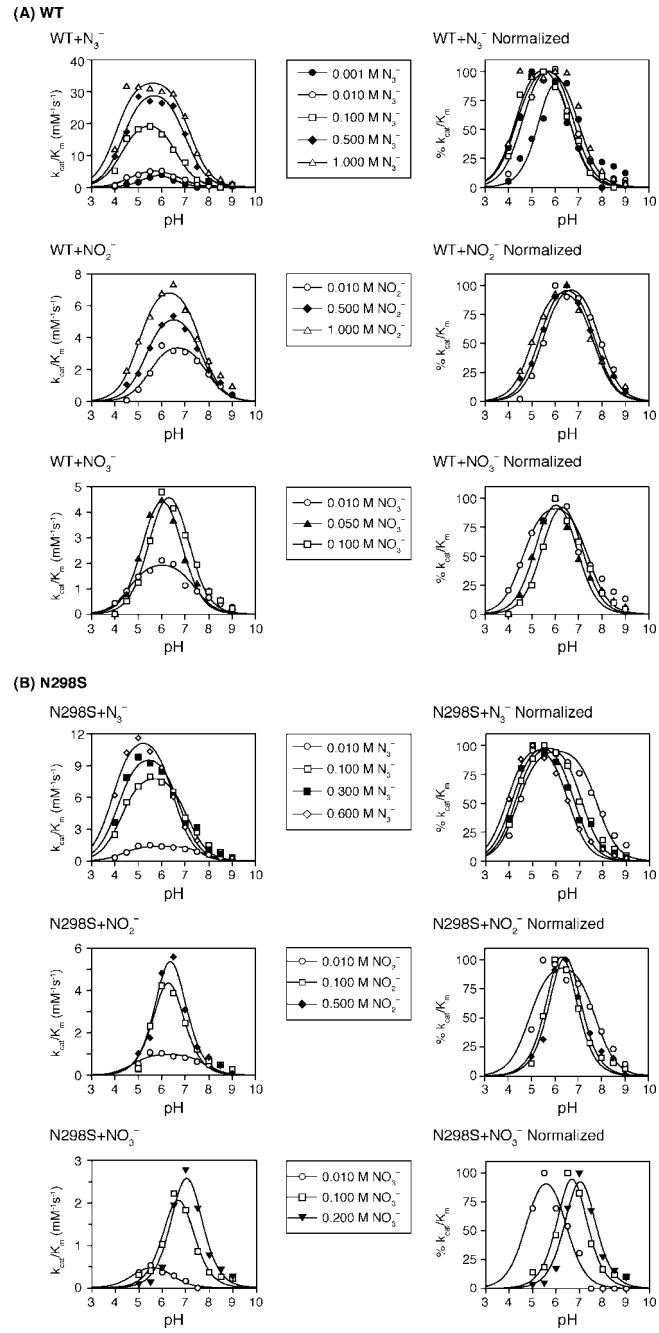

FIGURE 2: pH dependence of catalysis for (A) wild-type and (B) N298S variant HPA in the presence of the alternative anions, nitrite, nitrate, and azide, using CNP-G3 as the substrate. In each case, the pH dependence of k_{cat}/K_m on increasing anion concentration is plotted, along with the associated normalized curves. Derived pK_a values from these pH dependence curves are listed in Table 4. Related data for the naturally bound chloride anion can be found in ref *23*.

D197. Particularly noteworthy is the large decrease in pK_{a1} in the case of the azide anion.

Interestingly, for N298S variant HPA, the results obtained are less consistent, perhaps as a result of the more open space available for anion binding and the loss of a liganding group, which allows for a wider range of bound anion conformations. For chloride-bound N298S HPA, pK_{a1} is substantially lower, indicating that the change of N298 to serine has a substantial impact on D197. The trend for pK_{a2} is also somewhat lower but, like that of the wild-type enzyme, is very dependent on chloride concentration. In contrast, for

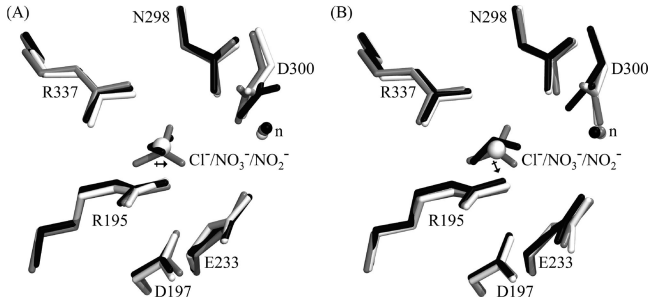

FIGURE 3: Composite drawing of the wild-type HPA chloride binding site region with bound activating chloride (white), nitrite (black), and nitrate (gray) in the (A) absence or (B) presence of the inhibitor acarbose. In addition, the direction of the dipole moment of bound nitrite is indicated by an arrow and is clearly sensitive to the presence of bound inhibitor in the active site. Residues directly within the chloride binding pocket (R195, R337, and N298) and nearby catalytic residues (D197, E233, and D300) are also drawn. The location of the water molecule believed to serve as the nucleophile in displacing covalent intermediates during substrate hydrolysis is indicated with the letter n. Most notably displaced upon anion exchange is the side chain of D300, when the nitrite anion is bound.

the nitrate and nitrite anions, the trend for pK_{a1} is to much higher values, with lower values for pK_{a2}, especially in the case of nitrite. Azide substitution effects are particularly unique for the N298S variant, with a pronounced decrease in pK_{a1} and pK_{a2}. As seen in Table 4, azide would appear to have the largest overall impact on the active site environment, in keeping with the largest differences being observed in substrate hydrolysis in the presence of this anion (Tables 2 and 3).

Structure of Nitrite-Substituted HPA. To probe the relationship between observed kinetic parameters for substitute anions and the binding modes of these in the chloride binding pocket, we have further determined the three-dimensional structures of HPA in the presence of the nitrite, nitrate, and azide anions using X-ray crystallographic techniques. For the nitrite anion, structural studies show that the normally resident chloride ion of HPA can be displaced by high concentrations of nitrite (400 mM) and that this alternative anion is found bound in the chloride binding pocket adjacent to the active site (Figure 3A). The presence of nitrite was initially confirmed via a difference electron density map covering the chloride binding pocket region. A well-defined, V-shaped peak of electron density was observed in this map, into which a nitrite ion was readily fit and refined at full occupancy. This apparent strong binding reflects the results of kinetic analyses, which indicate that HPA has a strong affinity for nitrite ion (Table 2), and its positioning in the chloride binding site near catalytic residues is consistent with this anion's ability to facilitate activation of catalysis in HPA (Table 3).

Relative to wild-type HPA, the main chain of the nitrite-containing structure exhibits an average rms positional deviation of 0.3 Å, indicating that the substitution of nitrite does not have a significant impact on the global fold of the enzyme. The principal areas of divergence involve small segments of flexible polypeptide chain localized to the exterior of the protein and exposed to solvent.

It is surprising from a structural perspective, given the polyatomic composition and unique planar geometry of nitrite, that this anion can be accommodated in the available binding pocket volume with remarkably little adjustment. Indeed, comparison of the wild-type and nitrite-substituted HPA structures indicates the close correspondence of the center of the nitrite anion and the position of bound chloride (Figure 3A). In this configuration, both the R195 and R337 chloride ligands remain key elements in facilitating and maintaining nitrite coordination, forming two hydrogen bonds each to this anion (Table 5). Even though the nitrogen atom of nitrite is ~0.5 Å closer to these ligands, little adjustment is observed in ligand conformations (Figure 3A). Like that in bound chloride ion, a further weaker interaction is made to the side chain of N298. In general, the larger overall size of the nitrite anion allows it to form hydrogen bond and electrostatic interactions stronger than those that are possible with chloride (Table 5).

Interestingly, bound nitrite has a dipole moment, and the negative end of this points toward the region of the active site cleft. As seen in Figure 3A, binding of this anion has little effect on the positioning of the catalytic residues D197 and E233. Overall, the most significant change in the placement of residues in or near the chloride binding pocket upon nitrite binding involves the third catalytic residue, D300. In particular, OD1 of the side chain of this residue is shifted by 1.0 Å, resulting in a hydrogen bonding pattern change, wherein D300 hydrogen bonds to the main chain carbonyl of H305 ($d = 2.8$ Å) and more weakly to ND2 of H299 ($d = 3.3$ Å). In wild-type HPA, D300 does not interact with H305 and instead OD1 interacts with a water molecule that is absent in the nitrite structure. In contrast, OD2 of D300 in both the wild-type and nitrite structures interacts with another water molecule in the active site region. Given these results, it would appear that changes in D300 positioning and interactions could be a major factor in kinetic and binding differences noted earlier upon nitrite substitution (Tables 2 and 3).

Nitrate-Substituted Wild-Type and N298S HPA Structures. Structural studies also show that the chloride of wild-type HPA can be displaced by high concentrations of nitrate (300 mM). This anion was initially localized to the chloride binding pocket via a difference map, which showed a well-defined trilobed peak of electron density. This anion was subsequently fit and refined at full occupancy. This difference map showed no other large peaks, indicating that nitrate binding did not have an impact on the overall global fold of HPA. Indeed, at the end of structural refinement, the main chain of the HPA−nitrate structure differed from that of wild-type HPA only by an overall average rms deviation of 0.1 Å. This is smaller than the average rms deviation of 0.3 Å between the main chains of the HPA nitrate- and nitrite-substituted structures.

Remarkably, the much larger nitrate anion fits within the chloride binding site with less perturbation than nitrite (Figure 3A). Indeed, no significant shifts of nearby ligand or active site residues were noted. Also absent is the shift in the side chain of D300 observed for the nitrite anion. Instead, interactions of the side chain of this residue in the nitrate structure closely parallel those of the chloride-bound wild-type enzyme (Table 5). Interestingly, nitrate binds within the chloride binding pocket with its oxygen atoms aligned in direct hydrogen bonding correspondence to the guanidinium groups of the side chains of R195 and R337, forming a pseudobicyclic ring structure (Figure 3A). Furthermore, the larger size of the nitrate anion means that it can form

Table 5: Anion Contact Distances

HPA structure	anion	atom	distance from anion to residue (Å)						
			R195 NE	R195 NH2	R337 NH1	R337 NH2	N298 ND2	E233 OE2	water
WT + Cl^-	Cl^-		3.23	3.34	3.45	3.14	3.38	5.00	3.44
WT + NO_3^-	NO_3^-	O1	−	2.83	−	−	−	3.59	−
		O2	2.88	−	2.92	3.56	−	−	−
		O3	−	−	−	2.65	3.07	−	−
WT + NO_2^-	NO_2^-	N	−	−	3.04	−	−	−	−
		O1	2.62	2.72	−	−	−	4.43	−
		O2	−	−	−	2.74	3.66	−	−
N298S + Cl^-	Cl^-		3.33	3.34	3.41	3.13	NA	5.01	3.21
N298S + NO_3^-	NO_3^-	O1	−	2.49	−	−	NA	3.57	−
		O2	2.81	−	2.67	3.42	NA	−	3.50
		O3	−	−	−	2.41	NA	−	−
WT + Cl^- + acarbose	Cl^-		3.23	3.41	3.26	3.43	3.41	4.97	3.32
WT + NO_3^- + acarbose	NO_3^-	O1	−	2.70	−	−	−	3.99	−
		O2	3.05	−	2.80	3.26	−	−	−
		O3	−	−	−	2.62	3.14	−	−
WT + NO_2^- + acarbose	NO_2^-	N	−	−	−	2.82	−	−	−
		O1	−	−	−	−	2.80	4.02	−
		O2	2.80	−	2.82	−	−	−	−
N298S + Cl^- + acarbose	Cl^-		3.21	3.42	3.38	3.16	NA	5.13	3.23
N298S + NO_3^- + acarbose	NO_3^-	O1	−	2.49	−	−	NA	3.57	−
		O2	2.64	−	2.63	3.11	NA	−	2.68
		O3	−	−	−	2.59	NA	−	−

stronger hydrogen bond and electrostatic interactions than are possible with either the normally resident chloride, or the substituted nitrite anions. This includes a much stronger hydrogen bond to the side chain of N298 ($d = 3.1$ Å) and a unique, although weak, direct interaction with the side chain of the catalytic residue E233 ($d = 3.6$ Å). The larger size of nitrate does, however, mean that in order to fit the binding pocket volume available, the center of this anion must be offset by 0.4 Å from that of a bound chloride ion.

The N298S variant of HPA has in the past proven to be a valuable asset in the study of chloride binding site properties, in that it has allowed for the examination of this site in the presence or absence of bound chloride (*23*). As such, this variant presents another window of opportunity for studying mechanistic aspects of this anion binding pocket, through the binding of substitute anions such as nitrate. To carry out this study, we have soaked the N298S variant in a high concentration of nitrate anion (300 mM) and with X-ray diffraction techniques shown that nitrate does indeed displace chloride anion in this variant structure. This has been confirmed with the use of difference electron density maps that indicate the positioning of nitrate in the chloride binding pocket at full occupancy and the further replacement of the side chain of N298 for that of a serine. No other significant difference map peaks were evident, and this, coupled with a 0.1 Å rms average deviation between the subsequent refined N298S nitrate−HPA structure and the same variant with bound chloride, indicates the similar fold of these two enzyme structures.

Figure 4 provides a comparison of the N298S HPA variant with and without bound chloride, and with bound nitrate anion. The greater volume of space available within the chloride binding pocket with the shortening of the side chain of residue 298 has allowed for a closer correspondence of the centers of the larger nitrate anion and that of chloride (0.1 Å vs 0.4 Å). Nonetheless, hydrogen bonding of nitrate in this modified pocket is similar to that found in the wild-type enzyme, involving a pseudobicyclic arrangement, which optimizes contacts with both the liganding side chains of R195 and R337 (Table 5). Absent, of course, is the interaction of nitrate-bound wild-type HPA with N298 (Figure 4).

Kinetic analysis of the N298S chloride- and nitrate-bound enzymes reveals significant differences in anion affinity [$K_d = 90$ and 39 mM, respectively (Table 2)]. These are both substantial increases in K_d compared to those of their wild-type counterparts ($K_d = 0.48$ and 0.80 mM, respectively)

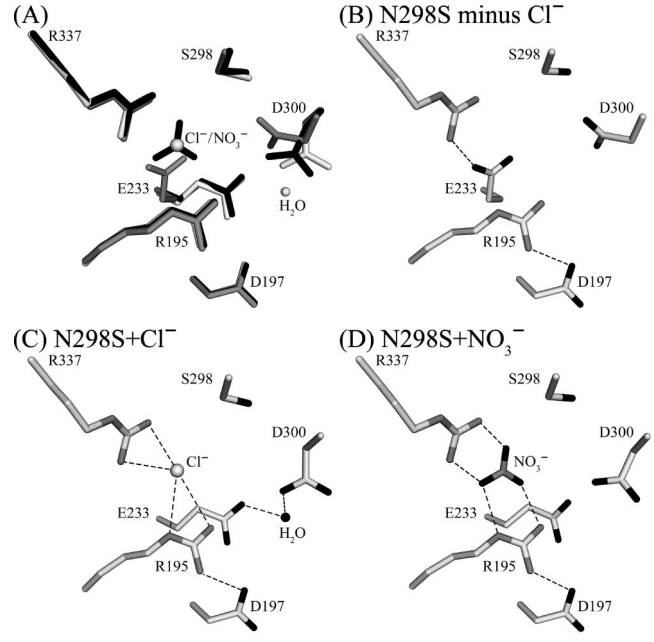

FIGURE 4: Frame A shows a composite drawing of three different structures determined for the chloride binding site of the N298S variant of HPA. In white shading, the naturally occurring chloride anion is bound; in the structure with gray shading, this chloride anion has been removed, and in the black-shaded structure, a substitute nitrate anion has been introduced. Details of anion hydrogen bonding in these three structures are shown in frames B−D, along with the positions of nearby water molecules. Notably, the bound nitrate anion serves to maintain the conformation of the variant HPA chloride binding pocket, whereas when no anion is present, the side chains of catalytic residues E233 and D300 shift into this region.

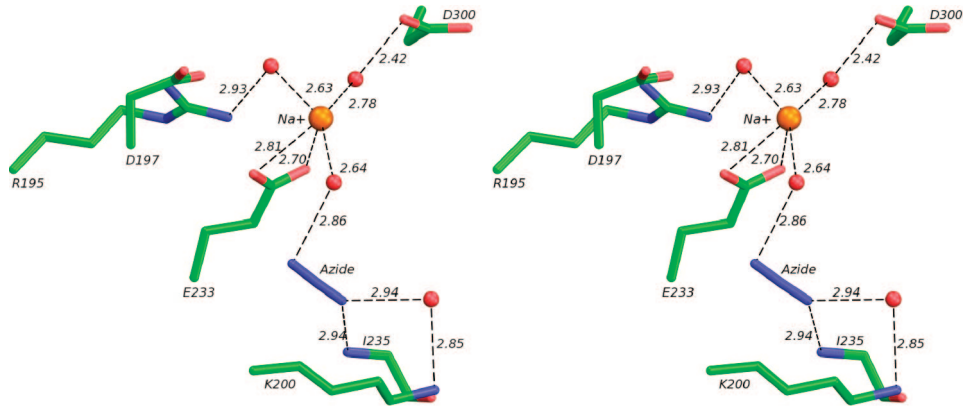

FIGURE 5: Stereo drawing illustrating the mode of azide (blue) binding within the active site of wild-type HPA. Unexpectedly, this anion does not bind in the chloride binding pocket where chloride is found under these conditions. Azide binding is localized to a well-defined pocket embedded in the surface of the substrate binding cleft, and it forms a primary electrostatic interaction with the charged side chain of K200. In wild-type HPA, this pocket is occupied by a water molecule, which is an important element in hydrogen bonding substrates and inhibitors (*31*). Also observed upon azide binding is the coordination of a sodium cation (orange) to E233 and, through a water molecule, to D300. Water molecules are shown as red spheres. Hydrogen bonds are designated with dashed lines, and observed bond distances are indicated.

and are undoubtedly due to the larger binding pocket space available and the loss of the N298 liganding interaction (*23*). Notably, the increase in K_d for nitrate in the N298S variant is much smaller in magnitude compared to that observed for chloride. This result is likely linked to the unique structural properties of the nitrate anion, namely, its much larger size and its ability to form closer contacts with the anion binding ligands R195 and R337 (Table 5). This, in turn, correlates with stronger electrostatic interactions than can occur with chloride, which act to retain nitrate in the bound state.

Interestingly, whereas nitrate binding in wild-type HPA allowed for the conservation of catalytic residue positioning, the N298S variant exhibits pronounced differences in the positions of key catalytic residues (Figure 4). Previous studies of the chloride-containing variant demonstrated that a water molecule takes the place of the shortened N298 side chain (*23*). This additional water molecule, which is hydrogen bonded to chloride, allows for the preservation of the positioning of D300 in its wild-type conformation. This result is not observed with nitrate binding, and inspection of this structure indicates that the larger size of this anion precludes binding of a similar water molecule. As a result, the side chain of D300 shifts away from its wild-type conformation toward the open space created by the substitution of N298 for a serine.

Another factor in catalytic residue shifts may involve the unique electrostatic environment created by nitrate binding. For this polyatomic anion, the strong interactions present to R195 and R337 likely result in the localization of its negative charge in the vicinity of these two residues. As a consequence, the opposite end of this anion, which is adjacent to the catalytic residues D300 and E233, would become more electropositive. This in turn would serve to attract the negatively charged side chains of both D300 and E233, drawing them closer to the nitrate. From a structural perspective, this is exactly what is observed (Figure 4), although the movement of D300 is also influenced by other factors as well, as discussed previously. Note that in the N298S variant when chloride is present, the position of E233 is unaffected. The influence of the modified electrostatic environment projected by a nitrate anion can also be seen in the lower apparent pK_a of E233 (Table 4).

Wild-Type and N298S HPA Structures with Bound Azide. Unexpectedly, our structural studies of wild-type HPA show that in the presence of high concentrations of azide anion (300 mM), the normally resident chloride ion remains bound in its binding pocket at full occupancy. Instead, initial difference electron density maps and subsequent structural refinements indicated that azide anions were bound at two alternative locations. One azide molecule is found in a solvent-exposed and shallow surface depression formed by a loop of polypeptide chain composed of residues 136–140. Beyond main chain hydrogen bonds, the primary electrostatic interaction made by this azide anion is to the charged side chain of K140. Two water molecules are also found closely associated with this bound azide. It seems unlikely that this azide anion is a factor in the dramatic enhancements in substrate HPA kinetic parameters noted earlier in the presence of this azide (Tables 2 and 3), given that the active site region is far removed from this binding site ($d > 20$ Å).

Likely of more relevance to catalytic parameters is a second azide molecule bound directly in the substrate binding cleft of HPA near active site residues. This azide anion is located in a well-defined pocket embedded in the wall of the region that forms substrate binding subsites +1 and +2, and as Figure 5 shows, a key electrostatic interaction that is formed is to the charged side chain of K200. As noted above, chloride remains bound to HPA under these conditions and is located ~9 Å from this second azide ion. Interestingly, azide binds to the opposite side of catalytic residues relative to the position of the bound chloride, with the closest approach being to the side chain of E233. Indeed, the side chain of E233 is almost perfectly sandwiched between these chloride ($d \sim 4.9$ Å) and azide ($d \sim 4.4$ Å) anions. This proximity to catalytic residues serves to explain the pronounced impact on pK_a values noted for E233 and D197 in Table 4.

Also found tightly bound in the active site region is a sodium ion, presumably originating from the high levels of sodium azide used to soak HPA in this experiment. This cation is directly coordinated to the carboxyl group of the side chain of E233 (Figure 5) and further interacts with the side chain of another catalytic residue, D300, through a hydrogen-bonded water molecule. Notably, this sodium ion is located almost exactly where hydrolysis is expected to occur for natural substrates. Given its prominent position near catalytic residues, there is the possibility that sodium ion

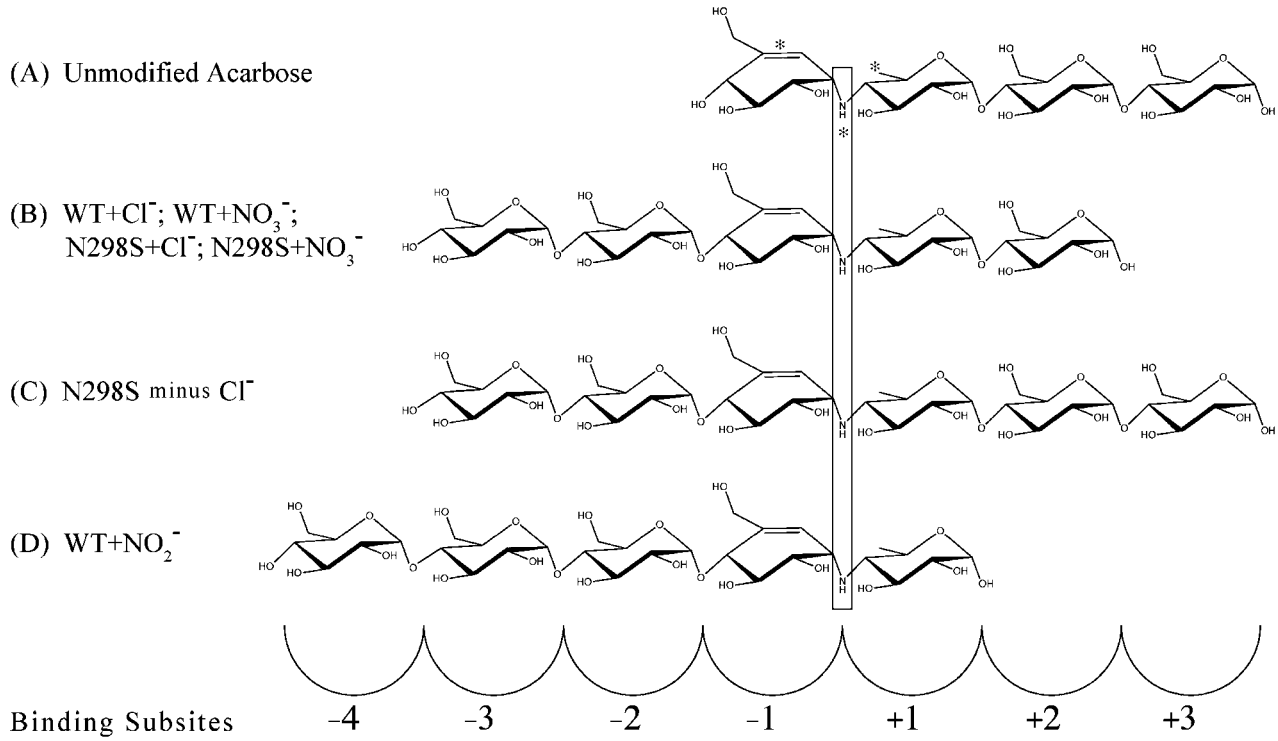

FIGURE 6: Line A illustrates the chemical structure of the HPA inhibitor acarbose and its expected binding mode if it were to be bound unaltered by HPA. The acarviosine group of acarbose has three unique features (denoted with asterisks) that include a distorted unsaturated ring species, a methyl group in place of an exocyclic hydroxymethyl group, and an N-linked glycosidic bond. Given its mimicry of the initial catalytic transition state of hydrolysis, this acarviosine group is expected to bind across subsites –1 and +1, between which cleavage of substrates would normally occur. As expected, HPA cannot cleave the N-linked glycosidic bond of acarbose but instead rearranges acarbose through a series of hydrolysis and condensation steps at other bonds to arrive at an inhibitor product with the acarviosine group bound in the expected –1 and +1 binding subsites. Line B shows the actual inhibitor product formed by rearrangement in chloride or nitrate-activated HPA, and in the chloride or nitrate-activated N298S variant, as well as the observed binding modes. Lines C and D show the unique products formed in the absence of any activating anion in the N298S variant and in the case of nitrite-activated HPA, respectively.

might play a role in the as yet unknown mechanism of azide activation of substrate hydrolysis. From this position, this sodium ion is ~5 Å from bound azide. Interestingly, this azide replaces a water molecule that would normally help orient and bind to incoming substrate molecules. Like this water molecule, azide anion appears to be sufficiently recessed into the wall of the binding cleft to allow for the normal binding of substrates.

Similar results were obtained in structural studies of the complex of azide anion with the N298S variant of HPA, with comparable positioning of a remote azide molecule near the polypeptide chain loop formed by residues 136−140, and an additional azide bound directly in the vicinity of the active site region. Also similarly placed was a tightly bound sodium ion directly interacting with the side chain of E233. One notable difference, however, was in the conformation of the side chain of D300, which was found shifted by ~1.5 Å toward the bound chloride ion. This appears to be a consequence of the loss of a water molecule that is normally found to replace the shortened side chain of residue 298 in this variant and forms interactions with chloride, S298, and the side chain of D300. Movement of the side chain of D300 toward the chloride binding site is likely the result of both the flexibility of interactions in this area and the altered electrostatic environment induced by azide binding nearby. Coincident with these changes is the readjustment of the flexible loop formed by residues 301–306, which plays a role in binding substrates in the active site cleft. As Tables 2 and 3 indicate, these structural differences in the N298S variant azide complex do not appear to have a significant effect on the relative enhancement of substrate hydrolysis activation observed in the presence of azide anion.

DISCUSSION

The naturally occurring inhibitor acarbose can serve as an excellent and sensitive "reporter" molecule on the catalytic "health" of modified HPAs. When bound to wild-type HPA, acarbose is rearranged through a series of five hydrolysis and transglycosylation events to form a pseudopentasaccharide, which is then tightly bound in the active site cleft (*22*). As illustrated in Figure 6, this rearranged product spans subsites −3 to +2 in the substrate binding cleft of HPA, with the two rings of the acarviosine group positioned in subsites −1 and +1, between which the hydrolysis of substrates would normally occur. The N-linked "glycosidic" bond between the two rings of acarviosine makes this group resistant to hydrolysis, and the resultant complex is thought to resemble the catalytic transition state. Notably, in the case of a modified HPA, alterations in the composition of the acarbose product formed have the potential to provide substantial insight into the altered nature of the catalytic properties affected by such modifications.

Interchangeability of Chloride and Nitrate HPA Activation. The results obtained for nitrate-substituted HPA demonstrate the considerable plasticity of the chloride binding pocket in accommodating a wide variety of anions with minimal structural adjustments, even when these are substantially larger

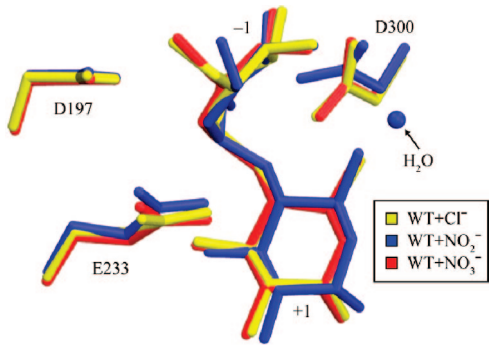

FIGURE 7: Overlay of the chloride-activated (yellow), nitrite-activated (blue), and nitrate-activated (red) HPA structures in the direct vicinity of the active site residues (D197, E233, and D300), when the inhibitor product derived from acarbose is bound. For clarity, only the acarviosine unit of acarbose is shown and the relevant +1 and –1 binding sites are labeled. Interestingly, in the nitrite-containing structure, the side chain of D300 shifts, allowing an additional water molecule to be directly bound in this region. Notably, the acarbose product formed during nitrite-activated catalysis is different from that observed for the chloride- or nitrate-activated reactions (see Figure 6).

than chloride and of a polyatomic nature. Further, the comparable kinetic parameters observed for the nitrate and chloride anions, in particular, indicate a similar mechanism of action in influencing active site residues during the hydrolysis of substrates (Tables 2 and 3). These results are in agreement with earlier studies (*15, 23*) that suggested the primary function of bound chloride is to shield the active site from R337 and thereby increase the pK_a of the catalytic residue E233. Our studies show that a large planar polyatomic anion like nitrate can carry out this function just as effectively.

Further evidence of the similarity of function of the chloride and nitrate anions is seen in structural studies of the HPA nitrate−acarbose complex, where first the nitrate anion retains a positioning similar to that of chloride in this complex [$\Delta d = 0.4$ Å (Figure 3B)] and there is retention of the conformations of nearby chloride binding site and catalytic residues. Second, the resultant acarbose product observed is the same as that obtained for wild-type HPA (Figure 6), indicating that nitrate-substituted HPA is capable of the same series of catalytic hydrolysis and transglycosylation steps. Our results further indicate a close similarity of acarbose product binding directly adjacent to catalytic residues (Figure 7) and in further removed binding subsites.

These results are in contrast to observations for the chloride-activated α-amylases of Gram-negative bacteria such as *Pseudoalteromonas haloplanktis*. For these enzymes, nitrate is an ineffective activator and there is the need for a focused negative charge such as chloride in the chloride binding pocket (*20*). These observations, coupled with the substantially different chloride binding pocket liganding interactions present, suggest that the functional roles of chloride binding in the bacterial and mammalian α-amylases are distinctly different and represent two different classes of enzyme.

The sensitivity of using a structure-based acarbose product assay approach to monitor the catalytic health of modified HPAs is amply illustrated for the N298S variant when chloride is alternatively present or absent. Earlier studies have shown that in the presence of chloride, there are some local changes in binding pocket and active site residue conformations, but that this modified enzyme is still capable of processing acarbose in the same fashion as wild-type HPA (*23*). In contrast, in the absence of chloride, much larger conformational changes are evident in enzyme groups and the resultant acarbose product obtained is different (Figure 6), indicating modified catalytic residue function.

The ability of nitrate to effectively substitute for chloride in HPA is further demonstrated in the case of the N298S variant nitrate−acarbose complex structure. As for the uncomplexed variant enzyme, nitrate and chloride occupy comparable positions (Figure 3), and as illustrated in Figure 6, the acarbose product obtained in either case is the same. This similarity extends to both acarbose product binding modes directly in the active site and in more remote binding subsites. Indeed, from a kinetic standpoint (Tables 2 and 3), the nitrate is more effective as an activating anion than chloride for this variant HPA. Our structural studies suggest this likely arises from a better fit of the larger nitrate ion within what is a much larger binding pocket in the N298S enzyme and a subsequent ability to more optimally align catalytic residues in the active site. This larger anion size would also seem to mitigate the effects of the loss of the normally present anion ligand to the side chain of N298.

Nitrite Substitution Substantially Modifies Catalytic Parameters and Product Profiles. In contrast to the results obtained for nitrate, in the HPA nitrite−acarbose complex a uniquely configured acarbose product is obtained (Figure 6), suggesting a strong modifying influence by nitrite anion on catalytic residues, cleavage preferences, and the pathway of hydrolysis and transglycosylation reactions occurring. For wild-type HPA, initial cleavage of acarbose is restricted to the bond between the two glucoses in the maltose unit, to yield acarviosine-glucose and glucose (*31*). The N-linked acarviosine group is inert to hydrolysis. The adjacent bond to glucose is also uncleavable likely due to the proximity of the acarviosine group and the fact that the absence of a 6-hydroxyl group on deoxyglucose is unfavorable for binding in the −1 subsite, where this missing hydroxyl would normally assist orientation of the catalytic nucleophile D197. As seen in Figure 6, the nitrite-substituted HPA has uniquely acquired the ability to cleave acarbose into its acarviosine and maltose groups. Furthermore, the acarbose product obtained is also unusually elongated at the opposite end to involve interactions in the −4 binding subsite.

Several additional observations from kinetic and structural analyses of nitrite-substituted HPA and the complex of this enzyme with acarbose are suggestive of the presence of significantly altered catalytic parameters. From a kinetic perspective, the boost in relative activity and k_{cat}/K_m values for nitrite (Tables 2 and 3) is surprising given structural studies that indicate a somewhat awkward fit of this anion in the chloride binding site in terms of hydrogen bond formation (Figure 3). This is particularly apparent on comparison of the elegant fit of the nitrate anion at this site, which fails to produce a corresponding increase in catalytic activity. This effect is even more pronounced for the N298S variant of HPA, with its much larger chloride binding pocket and which has one less liganding interaction. Here the nitrite replacement performs even better than its chloride or nitrate counterparts. One potential factor in this regard may be that the nitrite anion requires more spatial flexibility to optimally facilitate catalytic activity. Some support for this idea can

be seen in Figure 3, where it is evident that the orientation and dipole moment of bound nitrite are dependent on events occurring within the substrate binding cleft.

From a structural perspective, two notable changes are observed for nitrite-substituted HPA. As mentioned above, the first relates to how binding the acarbose product shifts the position (d = 0.4 Å) and orientation (~80°) of nitrite in the chloride binding pocket. As a consequence of this reorientation, the direction of the dipole moment of nitrite is redirected (Figure 3), thereby altering the electrostatic environment within its immediate vicinity. This environment is further modified by a change in hydrogen bonding pattern, wherein one nitrite hydrogen bond to the side chain of R195 is lost and a new one to the side chain of N298 is formed. As Table 4 indicates, the pK_a of D197 is substantially lowered in nitrite-substituted HPA, when compared to its chloride and nitrate counterparts, and this may serve to activate nucleophilic attack on substrates. The basis for this decrease in D197 pK_a may be grounded in the observed flexibility of nitrite to reorient its dipole moment and modify nearby hydrogen bond interactions in response to substrate binding.

A second significant structural change noted for nitrite-substituted HPA is in the orientation of the side chain of the catalytic residue D300. The interaction of D300 with O2 of the pyranose ring of a substrate in the −1 subsite is thought to alter the electronic configuration of the substrate in a manner that allows the oxocarbenium ion-like transition state, with its partially positive charge, to form (*11, 14*). As discussed in detail earlier, in the presence of nitrite anion the side chain of D300 shifts 1.0 Å away from the chloride binding pocket, leading to a change in the local hydrogen bonding pattern. An even more pronounced movement of this side chain is observed in the HPA nitrite−acarbose structure, when compared to the related wild-type enzyme complex. Particularly prominent is a 1.4 Å shift in the OD2 side chain atom of D300 (Figure 7), the displacement of which also alters nearby hydrogen bonding. In wild-type HPA, D300 hydrogen bonds to the NH group of the nonhydrolyzable bond of the acarviosine unit of acarbose, as well as to O2 and O3 of the pseudosaccharide in the −1 binding subsite (*22*). In contrast, the side chain of D300 in the nitrite-activated enzyme is now more than 4 Å from the nitrogen link of this inhibitor and instead hydrogen bonds to a new water molecule (d = 2.4 Å), which is not present in the wild-type HPA−acarbose complex (Figure 7).

Notably, the displacement of D300 in the active site of nitrite-substituted HPA would necessarily lead to the repositioning of substrates in the active site binding cleft next to catalytic residues. This may be the root cause for the unique ability of this modified enzyme to cleave maltose from the acarviosine unit of acarbose. Possible facilitators in this process would not only be a D300-induced altered orientation of substrates but also new interactions formed by the newly bound and novel adjacent water molecule found in the nitrite enzyme. In particular, these factors could promote a more optimal and flexible orientation of the D197 nucleophile, which is not as tightly dependent on interactions with the 6-hydroxyl of a glucose ring in the −1 subsite, a group missing when deoxyglucose binds at this site to lead to the generation of a maltose product from acarbose in nitrite-substituted HPA.

As exemplified by the unique acarbose product obtained from nitrite-substituted HPA (Figure 6), it is also apparent that this modified enzyme follows alternative hydrolysis and transglycosylation pathways in substrate processing with respect to those of the wild-type enzyme. Nonetheless, it is possible to propose how this might occur for acarbose rearrangement if one follows the example of wild-type HPA (*31*), coupled with the knowledge that the nitrite-modified enzyme can cleave maltose from this inhibitor and the reasonable assumption that maltose and glucose remain poor substrates. Further facilitating delineation of the most likely pathway followed is the fact that during the crystal soaking experiments used to elicit complex formation, the only substrates available to the nitrite-substituted HPA were acarbose and its cleavage products. As outlined in Figure 8, given these conditions, the simplest pathway for rearrangement would occur in five steps. Notably, the most likely steps involved are very different than the five-step process occurring for wild-type HPA rearrangement of acarbose (see Figure 8 in ref *31*). From Figure 8, it is also apparent that the cleavage specificity of nitrite-activated HPA is likely to be very different from that of wild-type HPA in a number of ways, and as an example of this,

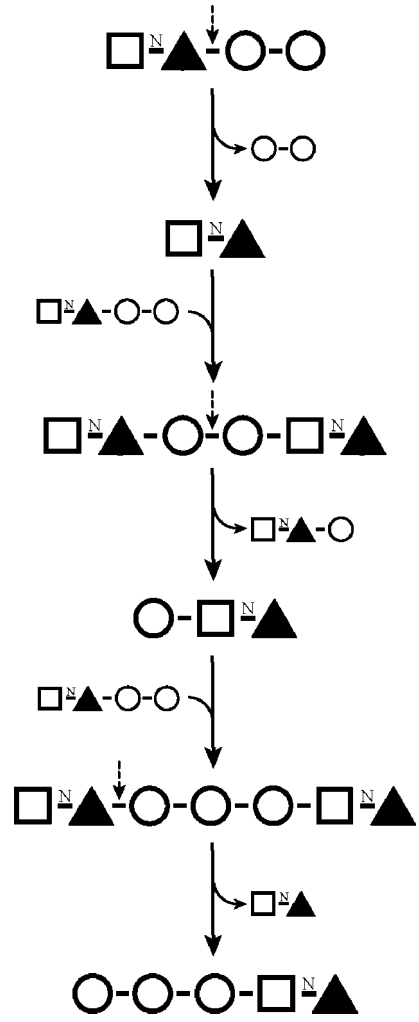

FIGURE 8: Proposed pathway for acarbose rearrangement in nitrite-activated HPA. This pathway begins with cleavage of the maltose group (O-O) from acarbose (□-▲-O-O) at the position of the dashed arrow. A new acarbose molecule then binds to the nonreducing end of acarviosine (□-▲) and forms a product having a maltose group in the middle and acarviosine at either end. This is cleaved between the glucoses of the maltose group. A third acarbose molecule then bonds to the product forming an intermediate with two acarviosine and three glucose units. The acarviosine at the nonreducing end is cleaved off to form the final product.

the final inert product formed would be readily cleaved in the presence of wild-type HPA.

Azide-Assisted Catalysis. The unexpected inability of azide to substitute for chloride in the active site of HPA, coupled with azide being found bound in an embedded side pocket in the substrate binding cleft, clearly suggests that the nature of the mechanism of azide-enhanced HPA catalytic activity is distinct from that observed for the nitrite and nitrate anions. Further clouding this issue is our inability to form and structurally characterize an HPA azide−acarbose complex, presumably because either azide binding leads to digestion of this inhibitor into products too small to bind to the enzyme surface or the placement of this anion in fact disrupts the normal course of acarbose binding. Nonetheless, the proximity of bound azide to nearby catalytic residues is suggestive of a direct role in catalysis, and it is apparent from Table 4 that this anion has a significant impact on the electrostatic environment of the active site. Indeed, its mechanism of action may well involve a contribution from the nearby and normally resident chloride ion, bound on the opposite side of the catalytic residue cluster. Regrettably, both what this alternative azide-assisted hydrolysis mechanism might be, and how to resolve this issue in future studies, remain unclear at this point.

ACKNOWLEDGMENT

We thank Christopher Overall, Yili Wang, and Chunmin Li for access to equipment and technical advice and Chris Tarling for helpful discussions.

REFERENCES

1. Berman, H. M., Westbrook, J., Feng, Z., Gilliland, G., Bhat, T. N., Weissig, H., Shindyalov, I. N., and Bourne, P. E. (2000) The Protein Data Bank. *Nucleic Acids Res. 28*, 235–242.
2. Brayer, G. D., Luo, Y., and Withers, S. G. (1995) The structure of human pancreatic α-amylase at 1.8 Å resolution and comparisons with related enzymes. *Protein Sci. 4*, 1730–1742.
3. Boel, E. L., Brady, A. M., Brzozowski, Z., Derewenda, G. G., Dodson, V. J., Jensen, S. B., Petersen, H., Swift, L., Thim, L., and Woldike, H. F. (1990) Calcium binding in α-amylases: An x-ray diffraction study at 2.1-Å resolution of two enzymes from *Aspergillus*. *Biochemistry 29*, 6244–6249.
4. Kadziola, A., Abe, J., Svensson, B., and Haser, R. (1994) Crystal and molecular structure of barley α-amylase. *J. Mol. Biol. 239*, 104–121.
5. Machius, M., Wiegand, G., and Huber, R. (1995) Crystal structure of calcium-depleted *Bacillus licheniformis* α-amylase at 2.2 Å resolution. *J. Mol. Biol. 246*, 545–559.
6. Ramasubbu, N., Paloth, V., Luo, Y., Brayer, G. D., and Levine, M. J. (1996) Structure of Human Salivary α-Amylase at 1.6 Å Resolution: Implications for its Role in the Oral Cavity. *Acta Crystallogr. D52*, 435–446.
7. Brzozowski, A. M., and Davies, G. J. (1997) Structure of the *Aspergillus oryzae* α-amylase complexed with the inhibitor acarbose at 2.0 Å resolution. *Biochemistry 36*, 10837–10845.
8. Tao, B. Y., Reilly, P. J., and Robyt, J. F. (1989) Detection of a covalent intermediate in the mechanism of action of porcine pancreatic α-amylase by using ^{13}C nuclear magnetic resonance. *Biochim. Biophys. Acta 995*, 214–220.
9. Braun, C., Brayer, G. D., and Withers, S. G. (1995) Mechanism-based inhibition of yeast α-glucosidase and human pancreatic α-amylase by a new class of inhibitors. *J. Biol. Chem. 270*, 26778–26781.
10. Rydberg, E. H., Sidhu, G., Vo, H. C., Hewitt, J., Côté, H. C. F., Wang, Y., Numao, S., MacGillivray, R. T. A., Overall, C. M., Brayer, G. D., and Withers, S. G. (1999) Cloning, mutagenesis, and structural analysis of human pancreatic α-amylase expressed in *Pichia pastoris*. *Protein Sci. 8*, 635–643.
11. Uitdehaag, J. C., Mosi, R., Kalk, K. H., van der Veen, B. A., Dijkhuizen, L., Withers, S. G., and Dijkstra, B. W. (1999) X-ray structures along the reaction pathway of cyclodextrin glycosyltransferase elucidate catalysis in the α-amylase family. *Nat. Struct. Biol. 6*, 432–436.
12. Zechel, D. L., and Withers, S. G. (2000) Glycosidase mechanisms: Anatomy of a finely tuned catalyst. *Acc. Chem. Res. 33*, 11–18.
13. Vasella, A., Davies, G. J., and Bohm, M. (2002) Glycosidase mechanisms. *Curr. Opin. Chem. Biol. 6*, 619–629.
14. Rydberg, E. H., Li, C., Maurus, R., Overall, C. M., Brayer, G. D., and Withers, S. G. (2002) Mechanistic analyses of catalysis in human pancreatic α-amylase: Detailed kinetic and structural studies of mutants of three conserved carboxylic acids. *Biochemistry 41*, 4492–4502.
15. Numao, S., Maurus, R., Sidhu, G., Wang, Y., Overall, C. M., Brayer, G. D., and Withers, S. G. (2002) Probing the role of the chloride ion in the mechanism of human pancreatic α-amylase. *Biochemistry 41*, 215–225.
16. Wakim, J., Robinson, M., and Thoma, J. A. (1969) The active site of porcine-pancreatic α-amylase: Factors contributing to catalysis. *Carbohydr. Res. 10*, 487–503.
17. Steer, M. L., and Levitzki, A. (1973) The metal specificity of mammalian-amylase as revealed by enzyme activity and structural probes. *FEBS Lett. 31*, 89–92.
18. Levitzki, A., and Steer, M. L. (1974) The allosteric activation of mammalian α-amylase by chloride. *Eur. J. Biochem. 41*, 171–180.
19. Feller, G., le Bussy, O., Houssier, C., and Gerday, C. (1996) Structural and functional aspects of chloride binding to *Alteromonas haloplanctis* α-amylase. *J. Biol. Chem. 271*, 23836–23841.
20. Aghajari, N., Feller, G., Gerday, C., and Haser, R. (2002) Structural basis of α-amylase activation by chloride. *Protein Sci. 11*, 1435–1441.
21. Parsons, D. S. (1971) Salt transport. *J. Clin. Pathol., Suppl. (R. Coll. Pathol.) s3–s5*, 90–98.
22. Brayer, G. D., Sidhu, G., Maurus, R., Rydberg, E., Braun, C., Wang, Y., Nguyen, N., Overall, C., and Withers, S. G. (2000) Subsite mapping of the human pancreatic α-amylase active site through structural, kinetic, and mutagenesis techniques. *Biochemistry 39*, 4778–4791.
23. Maurus, R., Begum, A., Kuo, H. H., Racaza, A., Numao, S., Andersen, C., Tams, J. W., Vind, J., Overall, C. M., Withers, S. G., and Brayer, G. D. (2005) Structural and mechanistic studies of chloride induced activation of human pancreatic α-amylase. *Protein Sci. 14*, 743–755.
24. Sambrook, J., Fritsch, E. F., and Maniatis, T. (1989) *Molecular Cloning: A Laboratory Manual*, Cold Spring Harbor Laboratory Press, Plainview, NY.
25. Leatherbarrow, R. J. (1998) *GraFit*, version 4.0, Erithacus Software Ltd., Staines, U.K.
26. Burk, D., Wang, Y., Dombroski, D., Berghuis, A., Evans, S. V., Luo, Y., Withers, S. G., and Brayer, G. D. (1993) Isolation, crystallization and preliminary diffraction analyses of human pancreatic α-amylase. *J. Mol. Biol. 230*, 1084–1085.
27. Otwinowski, Z., and Minor, W. (1997) Macromolecular crystallography, Part A. *Methods Enzymol. 276*, 307–326.
28. Brünger, A. T., Adams, P. D., Clore, G. M., DeLano, W. L., Gros, P., Grosse-Kunstleve, R. W., Jiang, J.-S., Kuszewski, J., Nilges, M., Pannu, N. S., Read, R. J., Rice, L. M., Simonson, T., and Warren, G. L. (1998) Crystallography & NMR system (CNS): A new software system for macromolecular structure determination. *Acta Crystallogr. D54*, 905–921.
29. Couture, A. M., and Laidler, K. J. (1956) The partial molal volumes of ions in aqueous solution. *Can. J. Chem. 34*, 1209–1216.
30. Oliver, B. G., and Campbell, A. N. (1969) Conductances, densities, and viscosities of concentrated solutions of lithium chlorate and of sodium chlorate in water-dioxane mixtures, at 25 °C. *Can. J. Chem. 47*, 4207–4211.
31. Li, C., Begum, A., Numao, S., Park, K. H., Withers, S. G., and Brayer, G. D. (2005) Acarbose rearrangement mechanism implied by the kinetic and structural analysis of human pancreatic α-amylase in complex with analogues and their elongated counterparts. *Biochemistry 44*, 3347–3357.

BI701652T